Supporting Information

Solvent-Regulated Mesoscale Aggregation Properties of Dilute pBTTT-C_{14} Solutions

Han L. Yi, Ching H. Wu, Chun I Wang, and Chi C. Hua*

Department of Chemical Engineering, National Chung Cheng University, Chiayi 62102, Taiwan, ROC

S1. Absorbance of pBTTT-C_{14} Solutions

The absorbance of pBTTT-C_{14} in two different solvent media was investigated using a commerical UV-vis spectrometer (JASCO, V-570). The measurement was conducted with cell having a path length of 2 mm (Hellma, 110-QS) to minimize the scattering associated with large pBTTT-C_{14} clusters. Figure S1 presents the results for two representative dilute solutions, with the wavelengths at the absorption maximum (λ_{max}) provided in Table S1. Both solvent systems of pBTTT-C_{14} show negligible absorption at the wavelength of incident light used in the present light-scattering experiment (λ = 632.8 nm). The pBTTT-C_{14}/toluene solution can be seen to exhibit a certain red-shift compared to the pBTTT-C_{14}/chlorobenzene solution, a phenomenon often attributed to

the effect of interchain aggregates or the formation of intrachain π-π stacking.[1,2] In addition, the shoulder at ~580 nm in the absorption spectrum is in close agreement with early report (~590nm)[3,4] for the contribution of intrachain $\pi-\pi$ association. Overall, the features in Figure S1 seem to support the notion that pBTTT-C_{14} forms rod-like aggregate (see discussion in the main text) mainly through $\pi-\pi$ stacking in toluene, whereas the chain pakcing assumes a less ordered state in chlorobenzene.

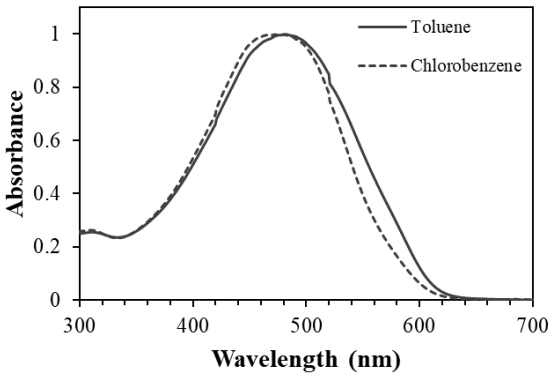

Figure S1. Absorption spectra of pBTTT-C_{14} in toluene (solid line) and chlorobenzene (dashed line) at 0.5 mg/mL and T = 25.0 ℃.

Table S1. Wavelengths at the Maximum Absorbance.

Solvent	λ_{max} (nm)
Toluene	483
Chlorobenzene	478

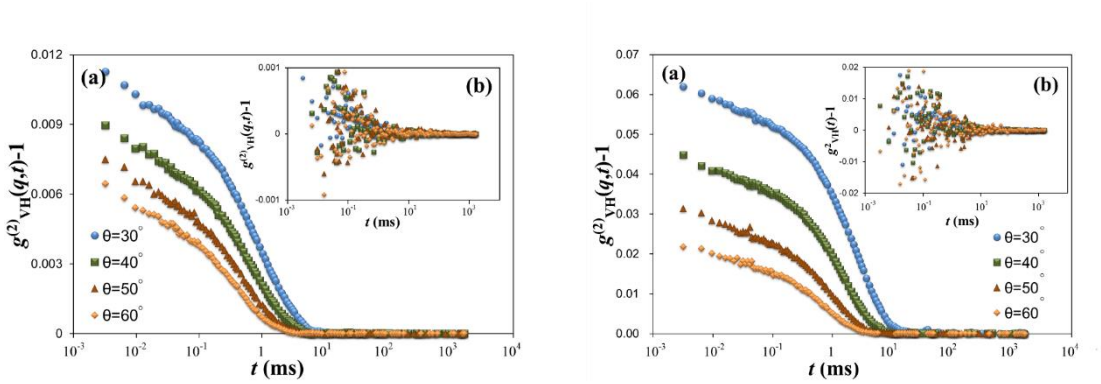

Figure S2. Intensity autocorrelation functions, $g^{(2)}_{VH}(q,t)$-1, in the DDLS experiment for pBTTT-C_{14} in (a) toluene and (b) chlorobenzene media at 0.5 (left) and 1.2 (right) mg/mL and T = 25.0 ℃, where different symbols represent the results from four different scattering angles.

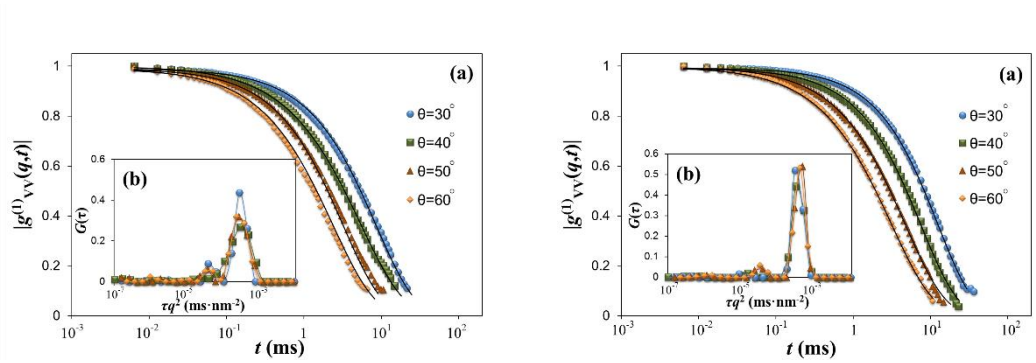

Figure S3. (a) Angular dependences of the field autocorrelation function, $|g^{(1)}_{VV}(q,t)|$, in the DLS experiment and (b) the relaxation time distributions, $G(\tau)$, retrieved from CONTIN as a function of τq^2 for pBTTT-C_{14}/toluene solutions at 0.5 (left) and 1.2 (right) mg/mL and T = 25.0 ℃. In (b), the fast mode corresponds to isolated small rods, and the slow mode represents cylindrical aggregate clusters. In (a), the full lines are nonlinear least-square fits according to eq 5.

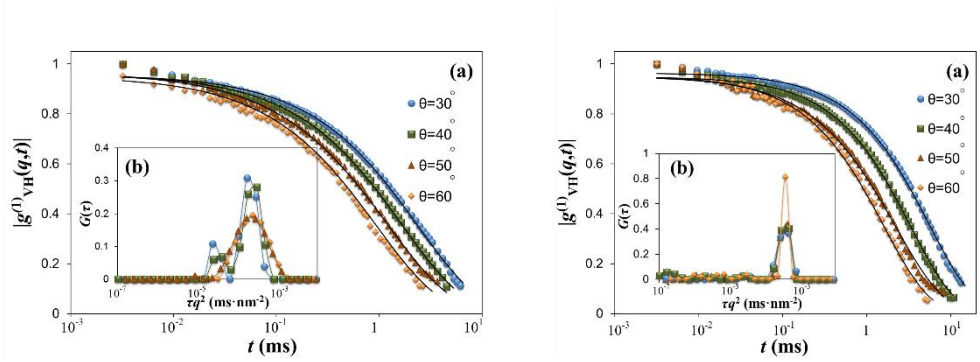

Figure S4. (a) Angular dependences of the field autocorrelation function, $|g^{(1)}_{VH}(q,t)|$, in the DDLS experiment and (b) the relaxation time distributions, $G(\tau)$, retrieved from CONTIN as a function of τq^2 for pBTTT-C_{14}/toluene solutions at 0.5 (left) and 1.2 (right) mg/mL and T = 25.0 ℃. In (b), the fast mode corresponds to isolated small rods, and the slow mode represents cylindrical aggregate clusters. In (a), the full lines are nonlinear least-square fits according to eq 6.

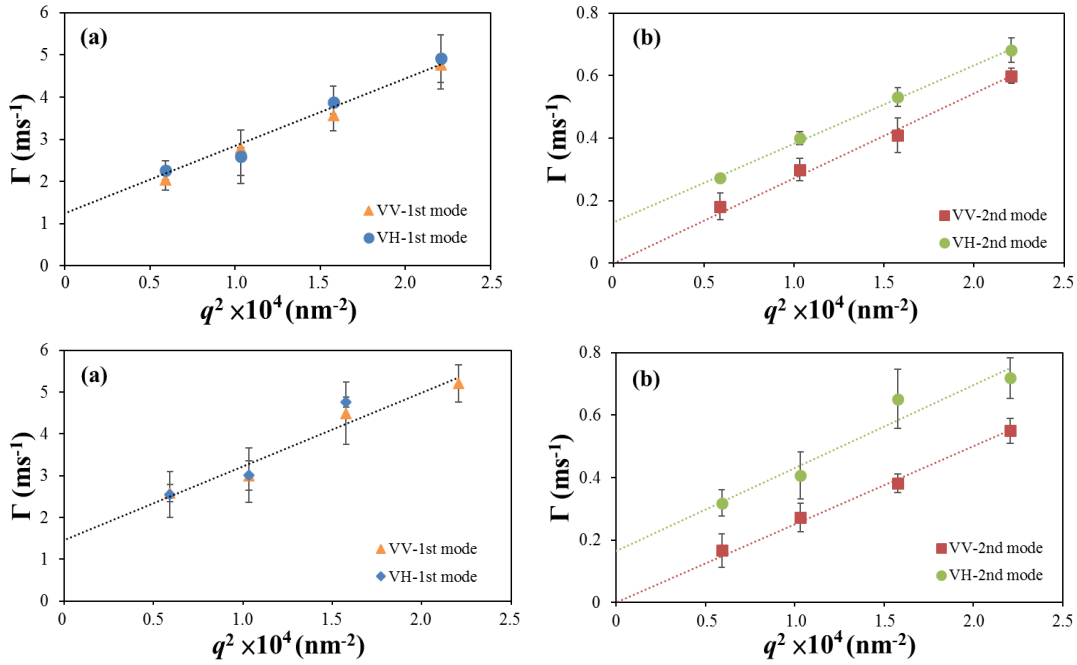

Figure S5. Mean decay rates, $\langle \Gamma \rangle$, as a function of q^2 for (a) the fast mode and (b) the slow mode for pBTTT-C_{14}/toluene solutions at 0.5 (top) and 1.2 (bottom) mg/mL and T = 25.0 ℃, where the dotted lines represent the results of linear regression.

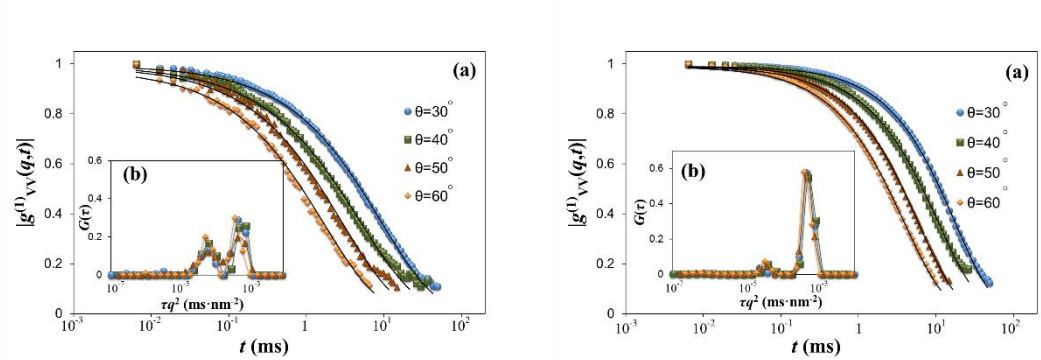

Figure S6. (a) Angular dependences of the field autocorrelation function, $|g^{(1)}_{VV}(q,t)|$, in the DLS experiment and (b) the relaxation time distributions, $G(\tau)$, retrieved from CONTIN as a function of τq^2 for pBTTT-C_{14}/chlorobenzene solutions at 0.5 (left) and 1.2 (right) mg/mL and T = 25.0 ℃. In (b), the fast mode corresponds to isolated small

rods, and the slow mode corresponds to spherical aggregates clusters. In (a), the full lines are nonlinear least-square fits using eq 15.

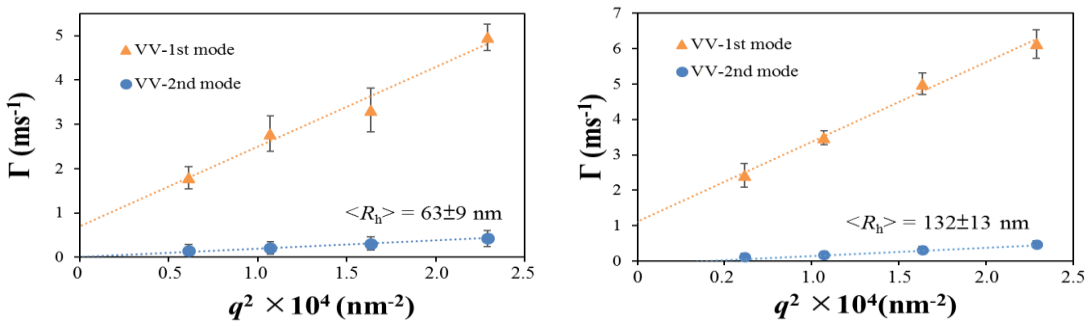

Figure S7. Mean decay rates, $\langle \Gamma \rangle$, as a function of q^2 for pBTTT-C_{14}/chlorobenzene solutions at 0.5 (left) and 1.2 (right) mg/mL and T = 25.0 ℃, where the dotted lines denote the results of linear regression.

S2. Description and Validation of the Force Field for AMD Simulations

For conjugated polymers, such as P3HT and pBTTT, there exist a few sets of force field describing the intramolecular and intermolecular interactions in the AMD simulation, especially for describing thermal-annealing condensed systems.[5-8] Considering the range of applications and, in particular, the transferability to include molecules other than the polymer itself, such as solvent and fullerene molecules, the OPLS (Optimized Potentials for Liquid Simulations)[9-11] seems ideal for this purpose. When compared to conventional flexible polymers, conjugated polymers bear relatively stiff chain conformation due to the alternate π-conjugation along the polymer backbone; therefore, adjustments of the backbone torsional potentials are often necessary. Recent studies have reported on several rational tactics to establish backbone torsional potentials by quantum chemical calculation along with a careful selection of the electron correlation methods and basis sets.[6,7,12,13] In this work, the density functional theory (DFT) scheme with long-range corrected B3LYP functional and 6-31+G** basis set is utilized for computing three different types of torsional potentials on the pBTTT-C_{14} backbone: the angle between thiophene and thiophene (T-T torsional angle, $\phi_{T\text{-}T}$), the angle between thiophene-thienothiophene (T-TT torsional angle, $\phi_{T\text{-}TT}$), and the angle between thiophene-side chain (T-S torsional angle, $\phi_{T\text{-}S}$), as illustrated in Figure S8a. All DFT calculations are conducted using a pBTTT-C_{14} monomer that is geometrically

optimized in the angular range of [-180°, 180°] with a scanning step of 18°. The computed profiles of the three torsional potentials are shown in Figure S8b-d. The potentials are then cast in the Ryckaert-Bellemans function: $U = \sum_{n=0}^{5} C_n[\cos(\phi\text{-}180°)]^n$, for which the parameters are listed in Table S2.

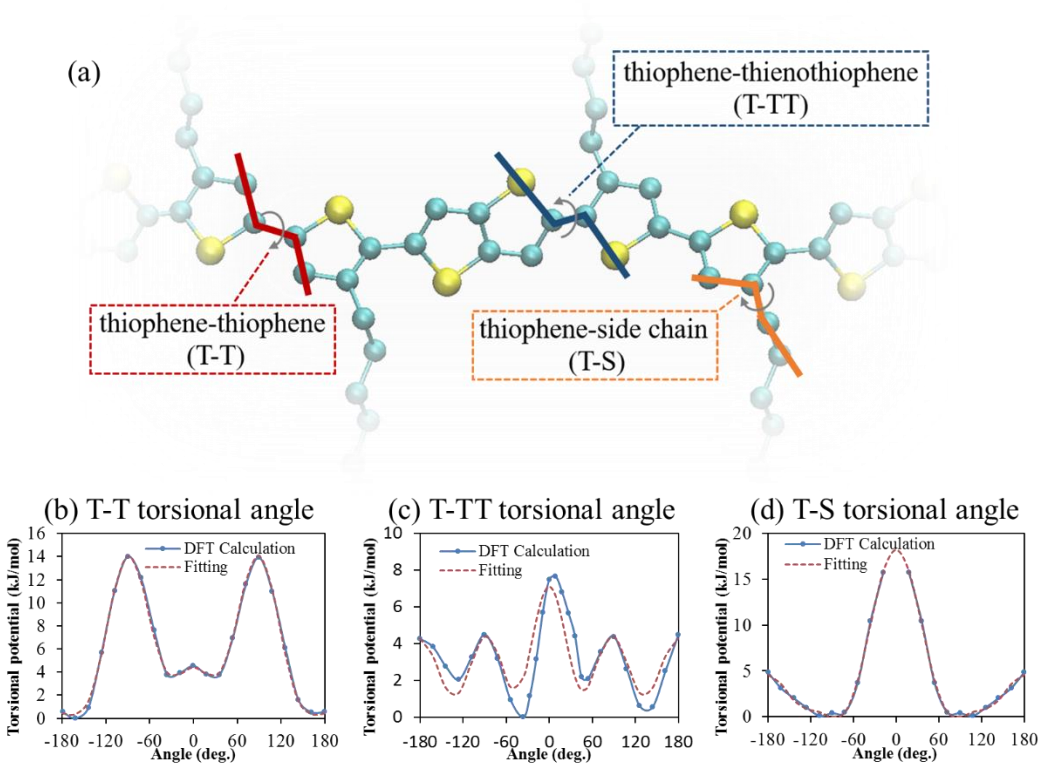

Figure S8. (a) Cartoons showing the thiophene-thiophene (T-T) torsional angle, the thiophene-thienothiophene (T-TT) torsional angle, and the thiophene-side chain (T-S) torsional angle; (b-d) profiles from the DFT calculation (blue) and the numerical fit (red) of each torsional potential function.

Table S2. List of Parmeters for the Potential Fuctions of Thiophene-Thiophene (T-T) Torsional Angle, Thiophene-Thienothiophene (T-TT) Torsional Angle, and Thiophene-Side Chain (T-S) Torsional Angle.

(kJ/mol)	T-T	T-TT	T-S
C_0	14.02720	4.37046	-0.10413
C_1	-1.23724	-1.12197	1.20116
C_2	-27.95620	-13.4778	4.69739
C_3	0.09482	3.91254	-12.7483
C_4	16.34800	14.7894	6.69424
C_5	-0.85083	-4.20482	4.72767

A further adjustment of the OPLS force field is on the partial atomic charges, which have a significant impact on intermolecular packing structures, i.e., the π-π staking. In the literature, there exist various schemes to derive partial atomic charges, such as Mulliken, NPA, AIM, CHELPG, Merz–Kollman, Resp, Hirshfeld, and GAPT.[14] These schemes often result in widely varying partial atomic charges, and there has been few systematic investigation into this issue.[15-18] In ref 15, Martin and Zipse suggested that partial atomic charges obtained from the CHELPG scheme with B3LYP/cc-pVDZ provide a relatively good prediction of the dipole moments for water molecule. Herein, the partial atomic charges on the backbone atoms of pBTTT-C_{14} are calculated in a similar manner, and the results are listed in Table S3. The partial atomic charges of the thiophene unit (No. 1−5 in Table S3) can be noted to be similar to the reported values for alkylthiophene oligomers.[6,19]

Table S3. List of Computed Partial Atomic Charges on the Backbone Atoms of pBTTT-C_{14} (the abbreviations C and S within the brackets referring to the carbon and sulfur atoms, respectively).

No. atom	Charge	No. atom	Charge	No. atom	Charge
1 (C)	0.056364	17 (C)	-0.00734	33 (C)	0.00031
2 (C)	-0.043491	18 (C)	0.08757	34 (C)	0.02932
3 (C)	-0.050626	19 (C)	-0.07000	35 (C)	-0.03062
4 (C)	0.062345	20 (C)	0.10179	36 (C)	-0.01116
5 (S)	-0.120155	21 (S)	-0.08463	37 (C)	0.08637
6 (C)	0.13061	22 (C)	-0.01679	38 (C)	-0.06671
7 (C)	-0.06502	23 (C)	0.03686	39 (C)	0.00086
8 (C)	0.00987	24 (C)	-0.14146	40 (C)	0.04636
9 (C)	0.05038	25 (C)	0.11383	41 (C)	0.00483
10 (C)	-0.04371	26 (C)	-0.01873	42 (C)	0.00771
11 (C)	-0.00428	27 (C)	-0.04266	43 (S)	-0.02918
12 (C)	0.03544	28 (C)	0.06812	44 (C)	0.04205
13 (C)	-0.02780	29 (C)	-0.04725	45 (S)	-0.03241
14 (C)	-0.00134	30 (C)	0.00405	46 (C)	-0.02409
15 (C)	0.03161	31 (C)	0.02902		
16 (C)	-0.03397	32 (C)	-0.02791		

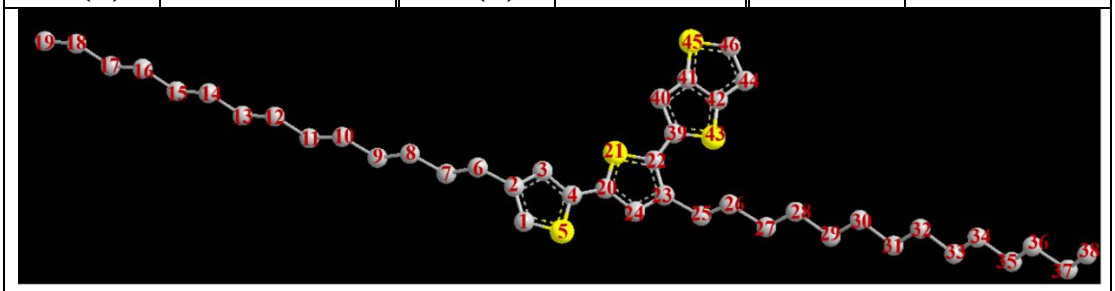

To verify the accuracy of the force field employed in this work, we have performed AMD simulation for a system of 28-chain pBTTT-C_{14}, each composed by 12 monomers or repeating units; the chains are arranged into 4 lamellae, with 7 π-π stacked chains on

each layer. A snapshoot of the resulting crystal structure is shown in Figure S9. The averge distance of π-π stacking and the lamellar spacing are found to be 4.15±0.34 Å and 18.09±1.46 Å, respectively, in good agreement with the experimental data from grazing incidence X-ray diffraction (GIXD) characterization.[20]

For solvent molecules, i.e., toluene and chlorobenzene, atomic interactions are described by the OPLS united-atom force field[9-11] along with partial atomic charges obtained from the CM4 charge model.[21] We have thoroughly evaluated and verified the force field employed in this work against known system density, self-diffusion coefficient, and viscosity of each solvent medium.[22]

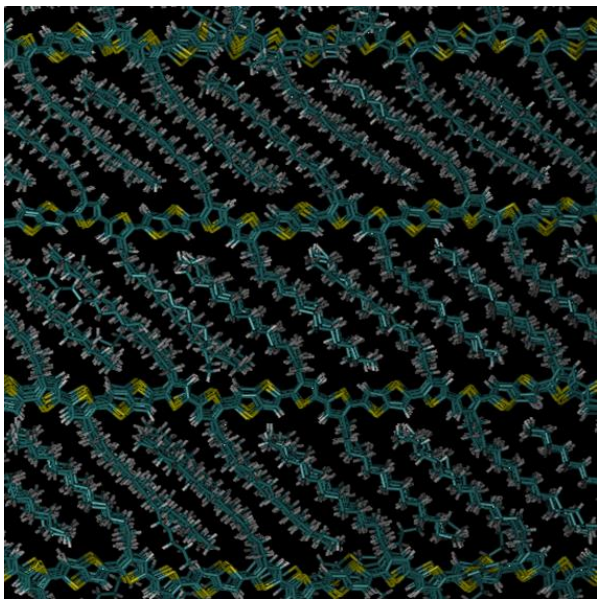

Figure S9. Snapshoot of a pBTTT-C_{14} crystal structure for validation of the force field employed in this work.

S3. Simulation Methodology

The AMD simulation is performed using the GROMACS package (version 5.1.2).[23] The equations of motion are integrated using the velocity Verlet algorithm with a time step of 1 fs. Periodic boundary conditions in all three directions are implemented. Long-range electrostatic interactions are treated using the smoothed-particle-mesh-Ewald (SPME) technique, with a precision of 10^{-5} and a real space cutoff of 12 Å. The same cutoff distance is used for the truncation of Lennard-Jones interactions, where standard geometric combining rules are adopted for any pair of unlike atoms. The general procedure of an AMD simulation is as follows: an isolated chain of pBTTT-C_{14} or their 5-chain aggregate is fixed in space and fully extended at the center of a cuboid box consisting of an appropriate number of solvent molecules, as listed in Table S4. The system is first equilibrated using *NPT* ensemble (with a coupling constant of 0.1 ps for both Nosé-Hoover thermostat and MTTK barostat) at 300 K and 100 bar for a duration of 100 ps to establish the initial condition. Afterward, the simulation is carried out at 1 bar and 300 K for 1 ns to help relax the changes due to the pressure adjustment. As the solution density of the simulation system properly converges, the single pBTTT-C_{14} chain and 5-chain pBTTT-C_{14} aggregate are then released to undergo free diffusion for another duration of 50 ns and 30 ns, respectively, when the data are recorded and utilized in the subsequent analyses.

Table S4. Description of the AMD Simulation System

Solvent medium	Single chain (12 monomers per chain)		Five-chain aggregate (12 monomers per chain)	
	No. solvent	No. chain	No. solvent	No. chain
T	10,560	1	13,374	5
CB	10,592	1	13,440	5

S4. Analysis Scheme of Interchain Order Parameter

To investigate the time-dependent chain packing of a pBTTT-C_{14} aggregate in the two solvent media, toluene and chlorobenzene, we have capitalized on the order-parameter (S) analysis for a pair of normal unit vectors, $\mathbf{n}_i$ and $\mathbf{n}_j$, located at the center-of-mass of the backbone rings on different chains, as shown in Figure S10. The order parameter, $S=P_2[\mathbf{n}_j(r)\cdot\mathbf{n}_i(r)]$ with P_2 being the second-order Legendre polynomial, serves as a measure of the spatial correlation of chain planarity and, hence, the degree of chain packing. The limiting values of P_2, 1, -0.5, and 0, correspond to parallel, perpendicular, and uncorrelated vectors, respectively. As shown in Figure 12 in the main text, the 5-chain aggregate in each solvent medium is initially arranged into perfect π-π stacking. Thus, in Figure S10, the order parameters of the thiophene-thiophene ($\mathbf{n}_1$-$\mathbf{n}_1$, $\mathbf{n}_2$-$\mathbf{n}_2$, and $\mathbf{n}_1$-$\mathbf{n}_2$) pairs and the thiophene-thienothiophene ($\mathbf{n}_3$-$\mathbf{n}_3$) pair bear a value of unity at this time. With increasing elapsed time and at small neighboring distances (r = 3.5−10 Å), interchain thiophene-thiophene pairs and thiophene-thienothiophene pairs are noted to sustain a high spatial order (S~1) in both solvent media. However, at large distances (r

> 10 Å), there is a profound difference in the dynamics of chain packing between the two solvent media. While the order parameters of thiophene-thiophene pairs and thiophene-thienothiophene pairs remain close to unity in toluene, they noticeably decay from unity to zero in chlorobenzene during the simulation. Thus, the order-parameter analysis provides clear evidence revealing that the 5-chain aggregate is able to sustain a highly ordered π-π stacking structure in toluene, whereas the previously arranged, ordered structure in chlorobenzene becomes notably disrupted later on and eventually disperses into separate isolated chains or smaller aggregates.

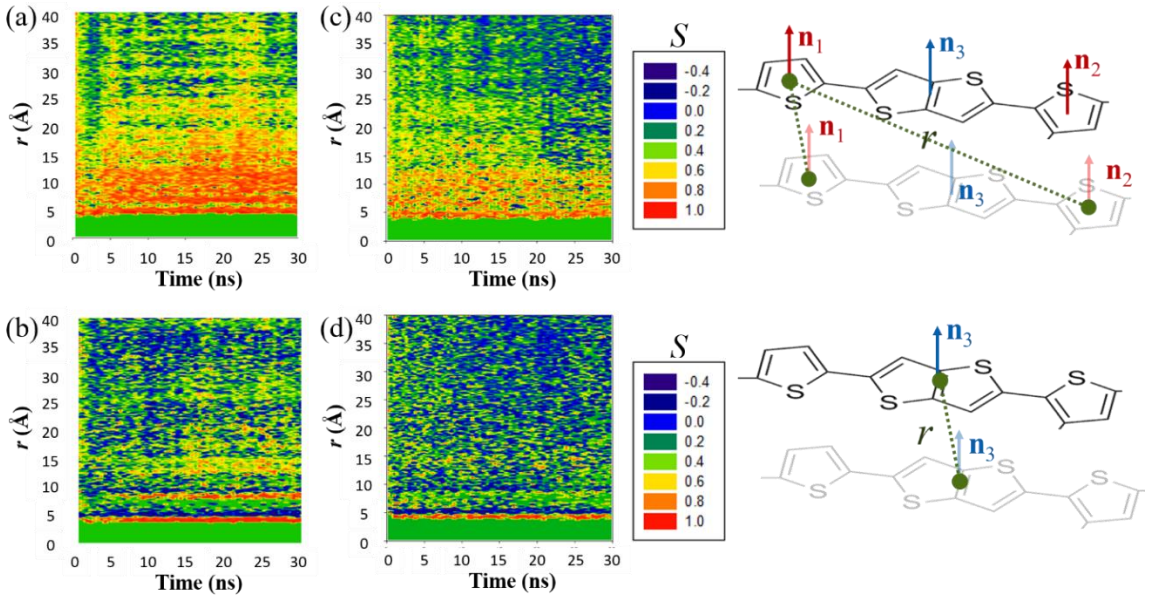

Figure S10. Time evolutions of the order parameters for different pairs of unit vectors normal to the chain backbone rings in (a-b) toluene and (c-d) chlorobenzene: the thiophene-thiophene pair (top) and the thienothiophene-thienothiophene pair (buttom), where the cartoons on the right panel show the corresponding pair alignment for the order-parameter analysis.

S5. Analysis Schemes of RDF and Torsional Conformation Relaxation for Single-Chain System

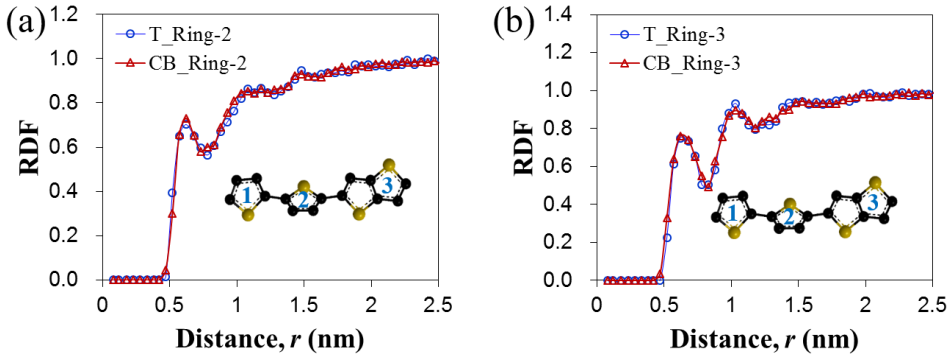

Figure S11. Radial distribution functions (RDFs) of (a) the solvent-thiophene (ring-2) pair and (b) the solvent-thienothiophene (ring-3) pair.

The relaxation dynamics of the backbone (torsional) conformation illustrated in Figure 13c is evaluated using the autocorrelation function: $\gamma(t) = < \mathbf{n}_i(t) \cdot \mathbf{n}_i(t_0) >$, where $\mathbf{n}_i$ is the normal unit vector of the i-th thiophene ring on the polymer backbone, and the angular brackets denote averaging over 50 independent time blocks along with the ensemble average of 12 monomers.

S6. Computational Insight into Light Scattering Analysis

The attribute of the fast mode in light scattering analysis of pBTTT-C_{14} solutions is of interest to know from the perspective of AMD simulations, especially for discriminating between small rod-like aggregates and—as previously suggested in the literature for pBTTT-C_n solutions—isolated chains. When viewed from the side-chain axis, the average diameter of a single pBTTT-C_{14} chain in both solvent media is estimated from the AMD simulation to be about 2 nm, which should be compared with the light scattering analysis indicating a diameter about 5 nm for the rod-like species. The recent work by Zhai's group suggested a folding conformation of pBTTT-C_{14} in specific crystalline conditions.[3,24] For the chain lengths investigated in the AMD simulation or in the light scattering analysis, however, it seems unlikely that chain folding might take place *in solution* due to the rigidity of the pBTTT-C_{14} backbone.

REFERENCES

(1) Wang, S.; Tang, J.-C.; Zhao, L.-H.; Png, R.-Q.; Wong, L.-Y.; Chia, P.-J.; Chan, H. S. O.; Ho, P. K.-H.; Chua, L.-L. Solvent Effects and Multiple Aggregate States in High-Mobility Organic Field-Effect Transistors Based on Poly(bithiophene-*alt*-thienothiophene). *Appl. Phys. Lett.* **2008,** *93*, 162103.

(2) Zhao, L.-H.; Png, R.-Q.; Zhuo, J.-M.; Wong, L.-Y.; Tang, J.-C.; Su, Y.-S.; Chua, L.-L. Role of Borderline Solvents to Induce Pronounced Extended-Chain Lamellar Order in π-Stackable Polymers. *Macromolecules* **2011,** *44*, 9692-9702.

(3) Hu, Z.; Liu, J.; Simón-Bower, L.; Zhai, L.; Gesquiere, A. J. Influence of Backbone Rigidness on Single Chain Conformation of Thiophene-Based Conjugated Polymers. *J. Phys. Chem. B* **2013,** *117*, 4461-4467.

(4) Zhang, Q.; Sun, Y.; Jiao, F.; Zhang, J.; Xu, W.; Zhu, D. Effects of Structural Order in the Pristine State on the Thermoelectric Power-Factor of Doped PBTTT Films. *Synth. Met.* **2012,** *162*, 788-793.

(5) Do, H.; Troisi, A. Developing Accurate Molecular Mechanics Force Fields for Conjugated Molecular Systems. *Phys. Chem. Chem. Phys.* **2015,** *17*, 25123-25132.

(6) Moreno, M.; Casalegno, M.; Raos, G.; Meille, S. V.; Po, R. Molecular Modeling of Crystalline Alkylthiophene Oligomers and Polymers. *J. Phys. Chem. B* **2010,** *114*, 1591-1602.

(7) Bhatta, R. S.; Yimer, Y. Y.; Perry, D. S.; Tsige, M. Improved Force Field for Molecular Modeling of Poly(3-hexylthiophene). *J. Phys. Chem. B* **2013,** *117*, 10035-10045.

(8) DuBay, K. H.; Hall, M. L.; Hughes, T. F.; Wu, C.; Reichman, D. R.; Friesner, R. A. Accurate Force Field Development for Modeling Conjugated Polymers. *J. Chem. Theory Comput.* **2012,** *8*, 4556-4569.

(9) Jorgensen, W. L.; Laird, E. R.; Nguyen, T. B.; Tirado-Rives, J. Monte Carlo Simulations of Pure Liquid Substituted Benzenes with OPLS Potential Functions. *J. Comput. Chem.* **1993,** *14*, 206-215.

(10) Jorgensen, W. L.; Maxwell, D. S.; Tirado-Rives, J. Development and Testing of the OPLS All-Atom Force Field on Conformational Energetics and Properties of Organic Liquids. *J. Am. Chem. Soc.* **1996,** *118*, 11225-11236.

(11) Jorgensen, W. L.; Schyman, P. Treatment of Halogen Bonding in the OPLS-AA Force Field: Application to Potent Anti-HIV Agents. *J. Chem. Theory Comput.* **2012,** *8*, 3895-3901.

(12) Bhatta, R. S.; Yimer, Y. Y.; Tsige, M.; Perry, D. S. Conformations and Torsional Potentials of Poly(3-hexylthiophene) Oligomers: Density Functional Calculations up to the Dodecamer. *Comput. Theor. Chem.* **2012,** *995*, 36-42.

(13) Raos, G.; Famulari, A.; Marcon, V. Computational Reinvestigation of the

Bithiophene Torsion Potential. *Chem. Phys. Lett.* **2003,** *379*, 364-372.

(14) Cramer, C. J. *Essentials of Computational Chemistry: Theories and Models;* Wiley & Sons, Inc.: New York, 2013.

(15) Martin, F.; Zipse, H. Charge Distribution in the Water Molecule—A Comparison of Methods. *J. Comput. Chem.* **2005,** *26*, 97-105.

(16) Okiyama, Y.; Watanabe, H.; Fukuzawa, K.; Nakano, T.; Mochizuki, Y.; Ishikawa, T.; Ebina, K.; Tanaka, S. Application of the Fragment Molecular Orbital Method for Determination of Atomic Charges on Polypeptides. II. Towards an Improvement of Force Fields Used for Classical Molecular Dynamics Simulations. *Chem. Phys. Lett.* **2009,** *467*, 417-423.

(17) De Proft, F.; Martin, J. M. L.; Geerlings, P. On the Performance of Density Functional Methods for Describing Atomic Populations, Dipole Moments and Infrared Intensities. *Chem. Phys. Lett.* **1996,** *250*, 393-401.

(18) Basma, M.; Sundara, S.; Ç algan, D.; Vernali, T.; Woods, R. J. Solvated Ensemble Averaging in the Calculation of Partial Atomic Charges. *J. Comput. Chem.* **2001,** *22*, 1125-1137.

(19) Marcon, V.; Raos, G. Molecular Modeling of Crystalline Oligothiophenes: Testing and Development of Improved Force Fields. *J. Phys. Chem. B* **2004,** *108*, 18053-18064.

(20) Cho, E.; Risko, C.; Kim, D.; Gysel, R.; Cates Miller, N.; Breiby, D. W.; McGehee, M. D.; Toney, M. F.; Kline, R. J.; Bredas, J.-L. Three-Dimensional Packing Structure and Electronic Properties of Biaxially Oriented Poly(2,5-bis(3-alkylthiophene-2-yl)thieno[3,2-b]thiophene) Films. *J. Am. Chem. Soc.* **2012,** *134*, 6177-6190.

(21) Rai, N.; Siepmann, J. I. Transferable Potentials for Phase Equilibria. 10. Explicit-Hydrogen Description of Substituted Benzenes and Polycyclic Aromatic Compounds. *J. Phys. Chem. B* **2013,** *117*, 273-288.

(22) Wang, C. I.; Hua, C. C. Solubility of C_{60} and Pcbm in Organic Solvents. *J. Phys. Chem. B* **2015,** *119*, 14496-14504.

(23) Abraham, M. J.; Murtola, T.; Schulz, R.; Páll, S.; Smith, J. C.; Hess, B.; Lindahl, E. GROMACS: High Performance Molecular Simulations through Multi-Level Parallelism from Laptops to Supercomputers. *SoftwareX* **2015,** *1–2*, 19-25.

(24) Liu, J.; Mikhaylov, I. A.; Zou, J.; Osaka, I.; Masunov, A. E.; McCullough, R. D.; Zhai, L. Insight into How Molecular Structures of Thiophene-Based Conjugated Polymers Affect Crystallization Behaviors. *Polymer* **2011,** *52*, 2302-2309.